Nuclear Instruments and Methods in Physics Research B 319 (2014) 71–74

Contents lists available at ScienceDirect

Nuclear Instruments and Methods in Physics Research B

journal homepage: www.elsevier.com/locate/nimb

Quantifying defects in N-layer graphene via a phenomenological model of Raman spectroscopy

Ronaldo Giro [a,*], Braulio S. Archanjo [a], Erlon H. Martins Ferreira [a], Rodrigo B. Capaz [a,b], Ado Jorio [c], Carlos A. Achete [a,d]

[a] Divisão de Metrologia de Materiais, Instituto Nacional de Metrologia, Qualidade e Tecnologia (Inmetro), Duque de Caxias, RJ 25250-020, Brazil
[b] Instituto de Física, Universidade Federal do Rio de Janeiro, Caixa Postal 68528, Rio de Janeiro, RJ 21941-972, Brazil
[c] Departamento de Física, Universidade Federal de Minas Gerais, Belo Horizonte, MG 30123-970, Brazil
[d] Departamento de Engenharia Metalúrgica e de Materiais, Universidade Federal do Rio de Janeiro, Caixa Postal 68505, Rio de Janeiro, RJ 21945-970, Brazil

ARTICLE INFO

Article history:
Received 21 January 2013
Received in revised form 23 October 2013
Available online 1 December 2013

Keywords:
Graphene
Ion bombardment
Computational simulation
Defects

ABSTRACT

We construct a model to obtain the density of point defects in N-layer graphene by combining Raman spectroscopy and the TRIM (Transport Range of Ions in Matter) simulation package. The model relates the intensity (or area) ratio of graphene's D and G bands to the defect density on each layer due to Ar^+ bombardment. Our method is effective for ion fluences ranging from 10^{11} to $\sim 10^{14}$ Ar^+/cm^{-2} and it should be in principle extendable to any kind of ion and energy.

1. Introduction

The presence of point defects in sp^2 carbon structures like graphite, graphene and carbon nanotubes (CNTs) is inherent to the synthesis processes such as growth and deposition, or it may be intentional. The intentional creation of defects aims to improve some properties of these materials like solubility or other physical–chemical property. For instance, acid treatment increases the water solubility and dispersion of CNTs in biological media by introducing oxidized carbon groups [1] making them efficient materials for detection and removal of pollutants in water [2,3]. The removal or addition of carbon atoms to CNTs has a dramatic impact on their electrical [4] and mechanical properties [5] and can be used to weld them together [6] or break them apart [7]. The electronic conductivity of graphene, in contrast with expectation, increases with increasing concentration of vacancy defects by more than one order of magnitude [8], and the mechanical properties are as strong as the pristine material [9].

In order to obtain the desired improvement in such materials properties, the amount of defects must be controlled and quantified. Raman spectroscopy has been largely used to identify defects in the sp^2-network of different carbon structures [10–13]. In a recent work, the evolution of the intensity ratio I_D/I_G between the disorder-induced D band ($1345\ cm^{-1}$) and the G band ($1585\ cm^{-1}$) with ion fluence was determined [14]. For monolayer graphene, being a strictly 2D material, it is straightforward to relate ion fluence to defect-density, thus providing a spectroscopy-based method to accurately quantify the density of defects of monolayer graphene. Following that work, Martins Ferreira et al. [15] showed that the same phenomenological formulas describing the evolution of I_D/I_G can also describe the ratio between integrated areas A_D/A_G in monolayer graphene.

Similar Raman data for N-layer graphene are available [16,15], but in this case the relation between ion fluence and the defect density on each layer is not straightforward, since it will certainly depend on factors such as ion mass, energy, and angle of incidence, which essentially determine the penetration depth. Therefore, to use Raman spectroscopy as a method to extract the depth-dependent defect density in a multilayer material, it is necessary to extend Lucchese's model [14] to multilayer graphene and to couple it to a method that simulates ion penetration profiles in graphene. This is the purpose of this work.

Our extended model (to be discussed) is coupled with TRIM package (Transport Range of Ions in Matter) [17–19] in order to obtain the density of defects in each graphene layer due to the ion bombardment. Our methodology is effective to describe the I_D/I_G and A_D/A_G ratios for ion fluence ranging from 10^{11} to $\sim 10^{14}$ Ar^+/cm^2. This methodology should be in principle extended to any kind of ion and energy.

* Corresponding author. Current address: IBM Research in Rio de Janeiro, Brazil. Tel.: +55 21 2132 3021.
E-mail addresses: rgiro@br.ibm.com, rgiro@ig.com.br (R. Giro).

0168-583X/$ - see front matter © 2013 Elsevier B.V. All rights reserved.
http://dx.doi.org/10.1016/j.nimb.2013.10.028

2. Model

The methodology used in this work is an extension of phenomenological model of Lucchese et al. [14]. In short, Lucchese et al. modeled the dependence of the intensity ratio (I_D/I_G) on the average distance between defects (L_D) by considering that a single impact of an ion on the graphene sheet causes a single defective structure responsible for modifications on two length scales, denoted by r_A and r_S (with $r_A > r_S$), where r_A and r_S are the radii of two circular areas measured from the impact point (see Fig. 1(a)). The area defined by r_S is the area where the impact of ion occurs, delimiting a structurally-disordered area named by Lucchese et al. [14] as S-region. For distances larger than r_S and shorter than r_A, the lattice structure is preserved, but the proximity to a defect causes a mixing of Bloch states near K and K' valleys of graphene Brillouin zone, leading to an enhancement of D band. This region was named as activated or A-region. If the Raman scattering process occurs at distances larger than $l = r_A - r_S$ from defective region, those regions will only contribute to the G band. According Lucchese et al. [14] the I_D/I_G ratio for a single graphene sheet is given by:

$$\frac{I_D}{I_G}(L_D) = C_A f_A(L_D) + C_S f_S(L_D) \quad (1)$$

where f_A and f_S are the fractions of A and S areas in the sheet, respectively, with respect to the total area. The A-regions contribute most strongly to the D band, while the S-regions make less contribution to the D band due to breakdown of the lattice structure itself. The analytical expressions for $f_A(L_D)$ and $f_S(L_D)$ are [14]:

$$f_S(L_D) = (1 - e^{-\pi r_S^2/L_D^2}) \quad (2)$$

$$f_A(L_D) = \frac{r_A^2 - r_S^2}{r_A^2 - 2r_S^2}(e^{-\pi r_S^2/L_D^2} - e^{-\pi(r_A^2 - r_S^2)/L_D^2}). \quad (3)$$

The parameters on Eq. 1 obtained in Ref. [14] are: C_A = 4.56, C_S = 0.86, r_A = 3 nm and r_S = 1 nm. Following this work, Martins Ferreira et al. [15] used the same expression Eq. 1 to fit the ratio between integrated areas A_D/A_G of Raman peaks (rather than the ratio between intensities) for a single graphene sheet. They fitted A_D/A_G ratio using different parameters [20]. In both cases the parameters were fitted for a laser energy of 2.41 eV (514.5 nm). For extension to others lasers, see Ref. [21].

A key to the model described above is the assumption that each ion causes a single defect, so one can readily identify the ion fluence Φ to the defect density σ and the typical distance between defects L_D, so $\Phi = \sigma = \frac{1}{\sqrt{\sigma}}$. This assumption breaks down for N-layer graphene, where a single ion can penetrate several layers and produce many defects, as shown schematically in Fig. 1(b). We now introduce a generalization of Eq. 1 for N-layer graphene, by averaging the contributions of each layer to I_D/I_G or A_D/A_G ratios:

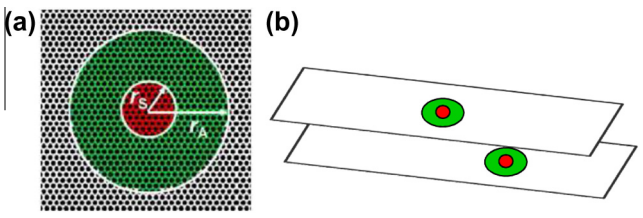

Fig. 1. (a) Definition of "activated" A-region (green) and "structurally-disordered" S-region (red). The radii are measured from impact point. (b) Extension of model (see text for details) for N-layer graphene sheets. (For interpretation of the references to colour in this figure caption, the reader is referred to the web version of this article.)

$$\frac{I_D}{I_G}(\Phi) = \frac{1}{N}\sum_{j=1}^{N} e^{-2\alpha z_j}[C_A f_A(L_{Dj}) + C_S f_S(L_{Dj})] \quad (4)$$

and similarly for A_D/A_G. In the expression above, N is the number of graphene layers, α is the light absorption coefficient for graphene/graphite (which depends on the laser wavelength used in Raman spectroscopy), L_{Dj} is the planar distance between defects in each graphene layer j (related to the defect density in each layer by $L_{Dj} = \frac{1}{\sqrt{\sigma_j}}$, z_j is the depth measured from the first graphene layer, and the factor 2 in the exponential is due to the optical length is twice the distance z_j of probed layer j). The exponential factor describes light attenuation in the N-layer graphene system. We use $\alpha = 1.583 \times 10^{-2}$ nm^{-1} corresponding to a wavelength of 514.5 nm [22]. It is implicit in Eq. 4 the assumption that contributions of D and G bands from each graphene layer are independent and additive, i.e., apparently a defect in a given layer does not modify significantly the contribution of another layer to the Raman signal.

In order to use Eq. 4, we need a method to obtain the density of defects on layer j (σ_j). For that, the well-established software TRIM (Transport Range of Ions in Matter), now called SRIM (Stopping and Range of Ions in Matter), based on Monte-Carlo simulations [17–19], was used to calculate the distribution of implanted Ar ions, vacancies, and sputtered ions and atoms from target (graphene) and substrate (quartz – SiO_2). To simulate the target and substrate, we use parameters (density, stoichiometry, displacement energy, surface binding energy and lattice binding energy) obtained from TRIM compound dictionary. The structural defects are produced by the simulation of collision between low energy (90 eV) Ar ions with the target and substrate. The ion beam incidence angle considered in this work was 45° with respect to the normal direction of the sample's surface [16,15]. The output of TRIM is the number of defects per ion ϕ_j in each layer j, and multiplication of ϕ_j by the ion fluence Φ (in units of ions/nm^2) gives the defect density on each layer σ_j. From σ_j we can extract the average distance between defects in graphene layer j as: $L_{Dj} = \frac{1}{\sqrt{\sigma_j}}$ [14]. From Eqs. 2, 3 and 4 we obtain the I_D/I_G ratio. Similarly for A_D/A_G ratio.

The parameters adopted to simulate N-layer graphene have to be carefully chosen. In particular, the displacement energy for carbon in graphene, reported in literature as 22 eV [23], is lower than that for bulk graphite (28 eV – from TRIM compound dictionary). This suggests a thickness dependence of this particular parameter. In order to address how a particular choice of parameters affects our main results and conclusions, we consider both values in our simulations.

3. Results and discussions

We first report the number of defects per ion calculated using TRIM for the specific conditions of the experiments, described in the previous Section: We find 0.76, 0.07 and 0.002 for the first, second and third graphene layers, respectively. In the fourth and deeper layers, graphene is intact, i.e., there is no defect due to ion bombardment. These values were obtained using the parameters from TRIM compound dictionary. When we consider the displacement energy for carbon atoms as 22 eV, the values obtained are 1.13, 0.22, 0.008 and 0.004 for the first, second, third and fourth graphene layers. In that case the fifth and deeper layers are intact.

We use these values to calculate the defect density in each layer and, subsequently, the I_D/I_G and A_D/A_G ratios, shown by the lines in Fig. 2(a) and (b), respectively, for graphene monolayer (1-LG), bilayer (2-LG), trilayer (3-LG) and 50 layers (HOPG). Solid lines are simulated results obtained using TRIM compound dictionary parameters, and dashed lines are the results obtained with just one different parameter: the displacement energy for carbon was

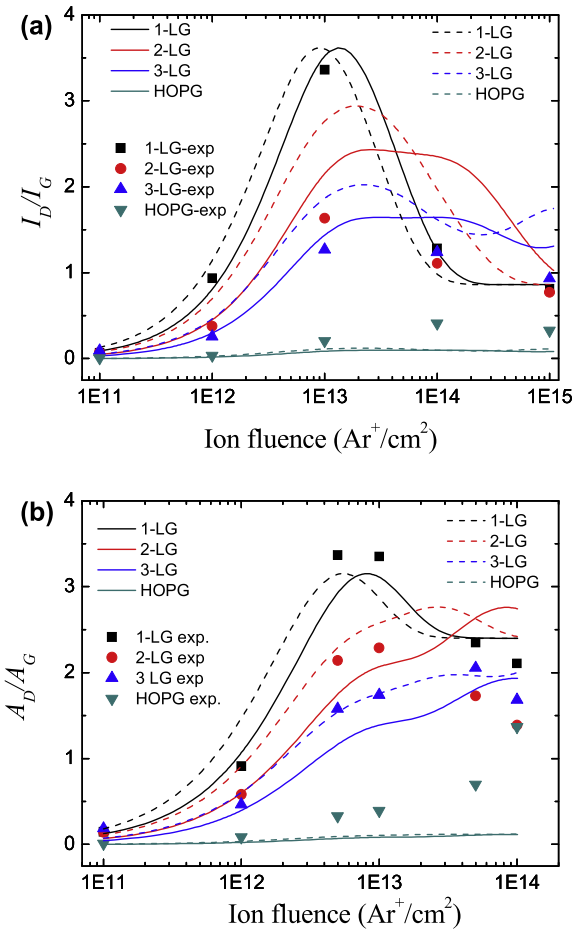

Fig. 2. Evolution of disorder in graphene as a function of the number of layers. (a) The D and G Raman band intensity ratios (I_D/I_G) are plotted as a function of ion bombardment fluence for 1-LG, 2-LG, 3-LG and 50-LG (HOPG). The lines result from our computational simulation and dots represent experimental results extracted from Ref. [16]. In (b), the ratios between integrated areas of the D and G bands (A_D/A_G) are plotted as a function of ion bombardment fluence for 1-LG, 2-LG, 3-LG and 50-LG (HOPG). Once again, lines are the results from simulations and dots are experimental results extracted from Ref. [15]. In both case (solid and dashed lines) the parameters: density, stoichiometry, displacement energy, surface binding energy and lattice binding energy are obtained from TRIM compound dictionary. For dashed line just one parameter is different: we consider the displacement energy for carbon in graphene as 22 eV, as reported in Ref. [23]

set to 22 eV (obtained from reference [23] for graphene). The corresponding dots represent the experimental data. We start discussing the results related to the former case, represent by solid lines. The different stages for the non-monotomic evolution of I_D/I_G [14] are clear in Fig. 2(a) – solid lines. This behavior is well established for 1-LG, while for 2-LG and 3-LG we see a distinct plateau after saturation of I_D/I_G ratio, ranging from 10^{13} to 10^{14} Ar$^+$/cm^2 ion fluence. This effect observed for 2-LG and 3-LG can be explained through the evolution of the defect density in each graphene layer, and the contribution of each graphene layer to the resulting I_D/I_G (see Eq. 4). When the first layer reaches the saturation of defects, and consequently the saturation of its contribution I_D/I_G ratio, the second layer still continues to contribute to increase I_D/I_G ratio since σ_j is one order of magnitude lower than in the first layer. The same argument is valid for 3-LG. For HOPG, a similar behavior is observed, but the plateau is not as clear due to the small values of I_D/I_G.

Fig. 2 – solid lines – also shows that the maximum I_D/I_G in most of cases occurs near $\sim 10^{13}$ Ar$^+$/cm^2 fluence; to be more precise at 1.3×10^{13} Ar$^+$/cm^2, 2.5×10^{13} Ar$^+$/cm^2, 2.9×10^{13} Ar$^+$/cm^2 and 1.1×10^{14} Ar$^+$/cm^2 fluence for 1-LG, 2-LG, 3-LG and 50-LG, respectively. The respective I_D/I_G values at those ion fluences are: 3.62, 2.43, 1.64 and 0.1. This result is consistent with Jorio et al. [16], as they stated that the maximum value of I_D/I_G scales roughly with the number of layers N.

Overall, results from computational simulations are in good agreement with experiments for 1-LG and 3-LG. For 2-LG, the agreement is worse for fluences larger than 1×10^{13} Ar$^+$/cm^2. For 1-LG and 3-LG, the agreement is better, and discrepancies occur for ion fluences higher than 10^{14} Ar$^+$/cm^2. In general, discrepancies for high fluences are expected because TRIM treats each ion impact as an independent event, and for high fluences the history of previous impacts plays an important role: As the number of defect sites increases substantially for high ion fluences, subsequent ion impacts have higher probability to find a region with a defect. These defective regions may act as tunnels, allowing ions to reach deeper graphene layers, increasing the density of defects in deeper graphene layers.

Similar trends can be seen in the evolution of the A_D/A_G ratio with ion fluence for 1-LG, 2-LG, 3-LG and 50-LG (HOPG), shown in Fig. 2(b) – solid lines. Interestingly, instead of the plateaus observed in the I_D/I_G plots, for 2-LG, 3-LG we observe a monotomic increase of the A_D/A_G ratio, with the presence of two distinct shoulders at ion fluences of $\approx 7 \times 10^{12}$ Ar$^+$/cm^2 and 7×10^{13} Ar$^+$/cm^2. However, the presence of these shoulders can be understood in a similar way as the presence of plateaus in the I_D/I_G plots.

We then compare the effect of different values for displacement energy for carbon. The results are shown in Fig. 2(a) and (b). Solid lines are the results obtained considering the displacement energy as 28 eV (obtained from TRIM compound dictionary for graphite), and dashed line as 22 eV (obtained from reference [23] for graphene). In both situations, I_D/I_G and A_D/A_G plots, the trends are very similar, although the values for I_D/I_G and A_D/A_G in dashed line plots are shifted to higher values in the range of low ion fluences: between 1×10^{11} and 1×10^{13} Ar$^+$/cm^2. For A_D/A_G there is a better agreement with experimental results for 3-LG (dashed line plot), and on the overall, solid and dashed lines shown quite similar results. It indicates that the A_D/A_G ratio is less sensitive to the difference between density of defects on each graphene layer obtained with different displacement energies for carbon. For I_D/I_G this is not the case. The good agreement with experimental results occurs only for 1-LG. One possible explanation is that, as far as the displacement energies are concerned, only the first layer behaves as graphene and deeper layers behave as graphite. As the second and deeper layers are sandwiched between two graphene layers, the interlayer interaction may enhance the threshold displacement energy with respect to a single graphene layer.

4. Conclusions

In summary, we extended the phenomenological model from Lucchese et al. [14] to describe the evolution of disorder as a function of ion fluence in N-layer graphene/graphite, for low-energy (90 eV) argon ions. Our method uses TRIM to obtain the density of defects on each graphene layer. There is good agreement between experiments and simulation for ion fluences lower than 10^{14} Ar$^+$/cm^2 for I_D/I_G ratio or lower than 10^{13} Ar$^+$/cm^2 for A_D/A_G ratio. Discrepancies for higher fluences are due to the assumption of independent events adopted by TRIM. The good agreement between simulation and experiment for low ion fluences suggests that this methodology could be extended, in this regime, to any kind of ion, energy, and varying incident angles. The method has very low computational cost and validates the use of TRIM to predict defect densities in such low-dimensional structures. The relatively good agreement between simulation and experiment also

validates the assumption that contributions of D and G different graphene layers can be added independently.

Acknowledgments

The authors thank the Brazilian agencies CNPq-PROMETRO, FAPERJ, FINEP, INCT – Nanomateriais de Carbono, and Rede Brasileira de Pesquisa e Instrumentação em NanoEspectroscopia Óptica for financial support.

References

[1] G.A. Umbuzeiro, V.R. Coluci, J.G. Honório, R. Giro, D.A. Morales, A.S.G. Lage, J.L. Mazzei, I. Felzenszwalb, A.G.S. Filho, D. Stéfani, O. Alves, Understanding the interaction of multi-walled carbon nanotubes with mutagenic organic pollutants using computational modeling and biological experiments, Trends Anal. Chem. 30 (2011) 437–446.
[2] X. Peng, J. Jia, Z. Luan, Oxidized carbon nanotubes for simultaneous removal of endrin and cd(π) from water and their separation from water, J. Chem. Technol. Biotechnol. 84 (2009) 275–278.
[3] G.D. Sheng, D.D. Shao, X.M. Ren, X.Q. Wang, J.X. Li, Y.X. Chen, X.K. Wang, Kinetics and thermodynamics of adsorption of ionizable aromatic compounds from aqueous solutions by as-prepared and oxidized multiwalled carbon nanotubes, J. Hazard. Mater. 178 (2010) 505–516.
[4] S. Lee, G. Kim, H. Kim, B.Y. Choi, J. Lee, B.W. Jeong, J. Ihm, Y. Kuk, S.J. Kahng, Paired gap states in a semiconducting carbon nanotube: deep and shallow levels, Phys. Rev. Lett. 95 (2005) 166402.
[5] R.W. Haskins, R.S. Maier, R.M. Ebeling, C.P. Marsh, D.L. Majure, A.J. Bednar, C.R. Welch, B.C. Barker, D.T. Wu, Tight-binding molecular dynamics study of the role of defects on carbon nanotube moduli and failure, J. Chem. Phys. 127 (2007) 074708.
[6] M. Terrones, F. Banhart, N. Grobert, J.-C. Charlier, H. Terrones, P.M. Ajayan, Molecular junctions by joining single-walled carbon nanotubes, Phys. Rev. Lett. 89 (2002) 075505.
[7] P.M. Ajayan, V. Ravikumar, J.-C. Charlier, Surface reconstructions and dimensional changes in single-walled carbon nanotubes, Phys. Rev. Lett. 81 (1998) 1437–1440.
[8] S.H.M. Jafri, K. Carva, E. Widenkvist, T. Blom, B. Sanyal, J. Fransson, O. Eriksson, U. Jansson, H. Grennberg, O. Karis, R.A. Quinlan, B.C. Holloway, K. Leifer1, Conductivity engineering of graphene by defect formation, J. Phys. D: Appl. Phys. 43 (2010) 045404.
[9] R. Grantab, V.B. Shenoy, R.S. Ruoff, Anomalous strength characteristics of tilt grain boundaries in graphene, Science 330 (2010) 946–948.
[10] R. Dillon, J. Woollam, V. Katkanant, Use of raman scattering to investigate disorder and crystallite formation in as-deposited and annealed carbon films, Phys. Rev. B 29 (1984) 3482–3489.
[11] A. Ferrari, J. Robertson, Interpretation of raman spectra of disordered and amorphous carbon, Phys. Rev. B 61 (2000) 14095–14107.
[12] L.G. Cançado, K. Takay, T. Enoki, M. Endo, Y. Kim, H. Mizusaki, et al., General equation for the determination of the crystallite size L_a of nanographite by raman spectroscopy, Appl. Phys. Lett. 88 (2006) 163106.
[13] B.S. Archanjo, A.P.M. Barboza, B.R.A. Neves, L.M. Malard, E.H.M. Ferreira, J.C. Brant, E.S. Alves, F. Plentz, V. Carozo, B. Fragneaud, I.O. Maciel, C.M. Almeida, A. Jorio, C.A. Achete, The use of a Ga^+ focused ion beam to modify graphene for device applications, Nanotechnology 23 (2012) 255305.
[14] M.M. Lucchese, F. Stavale, E.H.M. Ferreira, C. Vilani, M.V.O. Moutinho, R.B. Capaz, C.A. Achete, A. Jorio, Quanifying ion-induced defects and raman relaxation length in graphene, Carbon 48 (2010) 1592–1597.
[15] E.H. Martins Ferreira, M.V.O. Moutinho, F. Stavale, M.M. Lucchese, R.B. Capaz, C.A. Achete, A. Jorio, Evolution of the raman spectra from single-, few-, and many-layer graphene with increasing disorder, Phys. Rev. B 82 (2010) 125429.
[16] A. Jorio, M.M. Lucchese, F. Stavale, E.H.M. Ferreira, M.V.O. Moutinho, R.B. Capaz, C.A. Achete, Raman study of ion-induced defects in n-layer graphene, J. Phys.: Condens. Matter 22 (2010) 334204.
[17] J.F. Ziegler, M.D. Ziegler, J.P. Biersack, Srim – the stopping and range of ions in matter, Nucl. Instr. Meth. Phys. Res. B 268 (2010) (2010) 1818–1823.
[18] J. Ziegler, SRIM and TRIM – particle interactions with matter, 2012. <http://www.srim.org>
[19] J.F. Ziegler, J.P. Biersack, M.D. Ziegler, SRIM – The stopping and range of ions in matter, SRIM Co., Chester, Maryland, U.S.A., 2008.
[20] The parameters that describe the A_D/A_G ratio are $C_A = 3.6$, $C_S = 2.4$, $r_A = 4.1$ nm and $r_S = 2.6$ nm.
[21] L.G. Cançado, A. Jorio, E.H.M. Ferreira, F. Stavale, C.A. Achete, R.B. Capaz, M.V.O. Moutinho, A. Lombardo, T.S. Kulmala, A.C. Ferrari, Quantifying defects in graphene via raman spectroscopy at different excitation energies, Nano Letters 11 (2011) 3190–3196.
[22] G.E. Jellison Jr, J.D. Hunn, H.N. Lee, Measurement of optical functions of highly oriented pyrolytic graphite in the visible, Phys. Rev. B 76 (2007) 085125.
[23] J.C. Meyer, F. Eder, S. Kurasch, V. Skakalova, J. Kotakoski, H.J. Park, S. Roth, A. Chuvilin, S. Eyhusen, G. Benner, A.V. Krasheninnikov, U. Kaiser1, Accurate measurement of electron beam induced displacement cross sections for single-layer graphene, Phys. Rev. Lett. 108 (2012) 196102.